RESEARCH PAPER

# Effect of Alloying Elements on Hardness and Electrical Conductivity of Cu Nanocomposites Prepared by Mechanical Alloying

**Reza Mirahmadi Babaheydari\*, Seyed Oveis Mirabootalebi and Gholam Hosein Akbari Fakhrabadi**

*\* rezamirahmadi@uk.ac.ir*

Department of Materials Science and Engineering, Shahid Bahonar University of Kerman, Kerman, Iran

*Abstract: Cu-based alloys have a wide range of applications in the electronics industry, communications, welding industries, etc. Regarding the type and percentage of the second phase, changing in the alloying elements has a significant effect on the mechanical and electrical properties of copper composites. The aim of the present work is to synthesize, investigate, and compare the micro-structure, micro-hardness, and electrical properties of different Cu-based nanocomposites. For this purpose, Cu-Al, Cu-Al$_2$O$_3$, Cu-Cr, and Cu-Ti were fabricated via ball milling of copper with 1, 3, and 6 weight percentages. The vial speed was 350 rpm and the ball-to-powder weight ratio was kept at 15:1. The milling process was performed at different times in Argon. Next, the prepared composites were studied by scanning electron microscopy (SEM), X-ray diffraction (XRD), and dynamic light scattering (DLS). Based on XRD patterns, crystallite size, lattice strain, and lattice constant were calculated by Rietveld refinement using Maud software. The results show a decrease of crystallite size, and an increase of the internal strain and lattice constant by rising the alloying elements in all composites. The produced powders compressed via the cold press and annealed at 650 ℃. Finally; the micro-hardness and the electrical resistance of the manufactured tablets were measured. The results of these analyses show that the micro-hardness is increased by enhancement of the reinforcement material, due to the rising of the work hardening. Cu-6wt%Ti with 312 Vickers and Cu-1wt%Al$_2$O$_3$ with 78 Vickers had the highest and lowest micro-hardness, respectively. Moreover, the results of the electrical resistance indicate a dramatic rise in the electrical resistance by increasing the amount of alloying material, where Cu-1wt%Al with 0.26 Ω had the highest electrical conductivity.*

*Keywords: Copper Alloys, Mechanical Alloying, Electrical Resistivity, Mechanical Properties.*

## 1. INTRODUCTION

To modify the performance of copper nanocomposites, it is necessary to make a good balance between its electrical and mechanical properties. This means that Cu alloys should be strengthened without reducing their electrical properties [1-3] Increasing the mechanical properties through the formation of a saturated solid solution and the fine nanometer-scale sediments is always a suitable way to increase the strength, toughness, thermal stability, and creep resistance of copper; and at the same time, minimize the changes in the electrical properties of the Cu alloys [4-10]. A very good example here is Cu-Be alloys which has attracted very much attention by providing a strength of more than 1000 MPa and maintaining the electrical conductivity of copper. But the main drawback of this alloy, which has limited its industrial use, is the high cost and toxicity of beryllium [11]. Cu-Ti alloys are the best alternative to Cu-Be and some similar alloys, because of the high strength, corrosion resistance, high electrical

conductivities, and thermal stability [11, 12]. Similarly, each of the copper alloys has numerous properties and applications; for example, Cu–Al in memory alloys and solar powers [13], Cu-Al$_2$O$_3$ for electrode application [14], and Cu-Cr in fuel cells [15].

Different methods have been used to produce copper alloys. For instance, melting and casting processes [16], powder metallurgy [17, 18] severe plastic deformation (SPD) [19], sol-gel [20], and high-energy ball milling [21-26], are common methods for synthesizing Cu alloys. Among these, mechanical alloying (MA) due to simplicity, eco-friendly, cheapness of the process, and homogenous dispersion of the second phase, has a special place for the production of copper composites.

Concurrent variations in percentage and type of the second phase, because of changing the micro-structure and altering its electrical or mechanical properties, can reduce the accuracy of the applications of the Cu-based alloys. Several studies have been carried out by MA for production Cu alloys, but they just focus on

one type of copper alloy and none of them performed a comprehensive investigation on the simultaneous changes in the micro-structure, micro-hardness, and electrical conductivity of copper nanocomposite at different proportions of the second phase. In this study, different percentages of Al, $Al_2O_3$, Cr, and Ti used for synthesizing supersaturated solid solutions of copper by high energy ball milling. The fabricated nanocomposites were investigated by XRD, SEM and DLS analyses and the changing in the crystallite size, internal strain, the lattice constant, structure of the particles and particle-size distribution at different amount of the reinforce phases were investigated. Subsequently, heat treatment was performed and the hardness of the nanocomposite alloys was studied by the Vickers Micro-hardness test. Finally, the specimens were placed in an electrical circuit and their electrical resistance was measured.

## 2. EXPERIMENTAL PROCEDURES

Precursors were pure Cu (99.7%,<6μm), Cr (97%, <250μm), Al (97%,<45 μm), $Al_2O_3$ (97%,<75 μm), and Ti (97%,10 μm). Samples with three compounds of 1, 3, and 6 weight percentages of reinforcement materials milled in a planetary ball mill at Ar atmosphere. The initial amount of powders was 15 g, the balls were 10 and 15 mm in diameter. The ball-to-powder weight ratio was kept at 15:1 and rotational speed (vial speed) was 350 rpm. The milling time was 40 h for Cu-Al and Cu-$Al_2O_3$, and 90 h for Cu-Cr and Cu-Ti, respectively. Based on the previous studies [21, 27-29], the created solid solutions at similar conditions (e.g. milling time) with steel balls and vials had the highest micro-hardness.

The structural changes in obtained samples were studied by an X-ray diffractometer (Philips X'Pert, Cu-Kα, λ=0.1542 nm). Rietveld refinement was used to calculate the copper crystallographic parameters include lattice parameter, crystal size, and internal strain. In the Rietveld refinement, correction of the least-squares is performed until a suitable match is obtained between the observed pattern and the computational model. For calculation of the model, several parameters such as crystal structure, effects of diffraction, sample

properties, etc. are taken into account. The main feature of the Rietveld method is the ability to compare the obtained experimental XRD patterns with the information of structural models of different materials to estimate the crystal structure and percentage of formed phase. Furthermore, MAUD software, which has high accuracy in the calculation of crystallographic properties based on the Rietveld method, was used.

Morphology and size of ball-milled samples were analyzed by using scanning electron microscopy (Cam Scan mv2300) and the size distribution of samples was analyzed by zeta-seizer (ZEN3600). To sinter the mixed powders, the specimens were first molded to a diameter of 1 cm and thickness of 1 mm. Hence, 1.4 g of each alloy were pressed through a coaxial cold press machine (12 ton). Sintering process was carried out in a tube furnace for a half-hour at 650 ˚C in Ar. The Vickers microscopy test was performed according to the ASTM E 348-89 standard (Duramin20 Strues microprocessor) and micro-hardness was carried out with a force of 98.7 mN at 400 magnification for 5 s. The electrical resistance of the samples was measured by using an electrical circuit. The specimens were placed in the circuit and by applying a voltage, the electric current through the tablets was calculated. For more accuracy, the measurement was repeated 5 times on each sample and the mean values were reported. Afterward, the resistance of the samples was evaluated by Ohm's law [30].

## 3. RESULTS AND DISCUSSION

Fig. 1 shows the XRD patterns of Cu-1,3,6wt%Al, Cu-1,3,6wt%$Al_2O_3$, Cu-1,3,6wt%Cr and Cu-1,3,6wt%Ti after the ball milling process. By comparing the peaks, the highest and the lowest peak were observed in Cu-1wt%Ti and Cu-6wt%Cr, respectively. During the ball milling of copper alloys, powder particles are severely deformed by the impact of the balls which leads to an increase in the local temperature and as a result, atomic diffusion occurs. From the phase analysis point of view, solid solubility of Al in Cu is 9.4% at 567 ˚C and as the temperature decreases, the solubility of aluminum increases significantly [31, 32]. Conversely, the solubility of Cr and Ti

in Cu is very low at room temperature. The maximum solubility of Cr in Cu at a eutectic point is 0.82 atomic percentage and the maximum solubility of Ti in Cu is 8±1 atomic percentage at 885 ˚C [33-35]. Indeed, the XRD patterns show the superiority of the milling process in forming solid solutions at low temperatures.

At the same time, the density of crystalline defects such as vacancies, dislocations, and stacking faults were greatly increased during the process. Therefore, the particles work harden over time and with the increase in the work hardening the internal strain and the width of the peaks were also increased. The crystal defects are diffusion pathways for second phase atoms to dissolve in the copper matrix. On the other hand, after a long milling time and developing internal strains, the dislocations are regularly incorporated into the copper lattice and create subgrain boundaries. By continuing the milling process and increasing the density of the dislocations at the subgrain boundaries, they provide the basis for rotating these boundaries and convert them to the original boundaries [36, 37].

The increasing weight percentage of the reinforcement materials leads to reducing the intensity and broadening the width of the peak, and these peaks shift to lower angles (except $Cu-Al_2O_3$). Aluminum, chromium and, titanium have a bigger atomic radius than copper, therefore the dissolution of these elements and enhancement their concentration in the copper lattice, increases the copper parameter and shifts the peaks to lower angles. The none-displacement of the main copper peaks to the left or right indicates that the alumina particles are not dissolved within the copper lattice. Actually, they only were fractured and distributed in the copper matrix and so increases its local strain and grows dislocation density; in addition, this phenomenon leads to short and broad peaks.



**Fig. 1.** X-ray diffraction pattern of Cu-1,3,6wt%Al (a), Cu-1,3,6wt%Al₂O₃ (b), Cu-1,3,6wt%Cr (c) and Cu-1,3,6wt%Ti after ball milling procedure (d).

Fig. 2 provides information about the lattice constant of synthesized Cu-1,3,6wt%Al, Cu-1,3,6wt%Al$_2$O$_3$, Cu-1,3,6wt%Cr and Cu-1,3,6wt%Ti. It can be seen that by increasing the proportion of reinforcement material, expect for Alumina, the lattice parameter grows. Cu-Al, Cu-Cr, Cu-Ti, and Cu-Al$_2$O$_3$ had the highest lattice constant, respectively. The entrance of the large aluminum, chromium and titanium atoms in the copper matrix increases the copper lattice parameter and it is a sign of the formation of a solid solution. The high concentration gradient in the presence of large quantities of the reinforcement elements in the primary powder mixture will help the second phase atoms to diffuse in the copper lattice, therefore, a more saturated solid solution is formed. In fact, the possibility of collisions is increased by raising the proportion of reinforcement materials, thereby the lattice parameter grows. The reason for the lack of change in the Cu-Al$_2$O$_3$ lattice constant is non-diffusion of alumina particle within the copper lattice. However, if diffusion of the alloying elements occurs, the lattice parameter will continue to change, as Sheibani et al. report [38] lattice constant was increased in Cu-Cr alloy with a constant rate in the milling process.
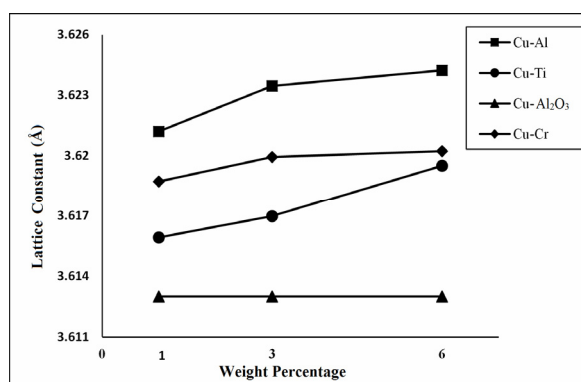


**Fig. 2.** Lattice constant of the produced samples.

The crystallite size of Cu-Al, Cu-Al$_2$O$_3$, Cu-Cr, and Cu-Ti with different reinforcement material percentages are shown in Fig. 3. Cu-1wt%Al$_2$O$_3$ has the largest crystalline size (32 nm), and Cu-6wt%Cr and Cu-6wt%Ti have the smallest crystalline size (9 nm).

Generally, the crystallite size is determined by the competition between plastic deformation through the motion of dislocations, and the recovery and recrystallization [39]. Indeed, recovery and recrystallization increase by reducing the plastic deformation, conversely, the crystallite size decreases. In this study, due to the low milling speed (350 rpm) and 15 min stop after 30 minutes of ball milling, the vial temperature did not increase and so the recovery and recrystallization phenomenon did not occur. As well as, the crystallite size was uniformly decreased alongside the increasing the plastic deformation. The higher initial proportion of alloying elements accelerates work hardening. Alloying particles were dissolved and as a result, the hardness of the matrix was increased because of the fraction, diffusion, and segmentation of crystallite during the ball-milling process [37]. The reason for the more reduction of the crystal size in the compositions with more fraction of aluminum, chromium, and titanium is the aggregation of the effect of cold working and saturation of the copper matrix. Moreover, by increasing the percentage of the reinforcement materials, the effects of the cold working become more apparent, and as a result, subgrain boundaries and dislocations are created more and more [21, 28, 37, 40].



**Fig. 3.** Crystal size of the samples after the milling process.

Fig. 4 shows the internal strain of the samples. Cu-Al$_2$O$_3$ and Cu-Al have the lowest and highest strain, respectively. Initial powders are strain-free, but by starting the milling process, a rapid increase in the number of dislocations and other crystallographic defects are created. Gradually, via the formation of dislocations and reaching the crystallite size to a few nanometers, the number of dislocations has reached the saturated extent and under this situation, no new dislocations created by increasing milling time. On the other hand, atoms of alloying elements have also entered into the Cu lattice during this

4

period; and so these two phenomena impose strains on the lattice of copper. As shown in Fig. 4, by increasing percentages of the second phase, the lattice strain of all samples is grown. In copper composites due to combination with the higher amount of reinforcement materials, the effects of cold working were much more severe, and the dissolutions of alloying elements are enhanced [41]. Consequently, the structure of the matrix is more affected owing to the cold working and more defects. Eventually, a much higher strain in the lattice is created. Copper-alumina, due to the non-dissolution of alumina in the copper lattice, has lower strain than other compounds. However, aluminum, chromium, and titanium by dissolving in the copper matrix and forming a solid solution, cause more strain into the copper lattice.



**Fig. 4.** Strain changes of the samples after the milling process.

The particle size distribution of the samples is shown in Figure. 5. Cu-1wt%Al$_2$O$_3$ and Cu-6wt%Al have the largest (954 nm) and the smallest (38 nm) particle size, respectively. According to Figure. 5, particle size are decreased as increasing the proportion of the second phase and creation of the richer solid solution, which has led to an expand the work hardening of the samples. Therefore, the samples with higher amounts of reinforcement materials were more fractured and the powder particles, due to the more work hardening of the solid solution, have a smaller size. It should be noted in all samples, some large particles of powder in the solution are deposited and the results illustrate the smaller particles. However, the important point in this analysis is proving the achievement of the micro-sized particles in Cu composites by the MA method.
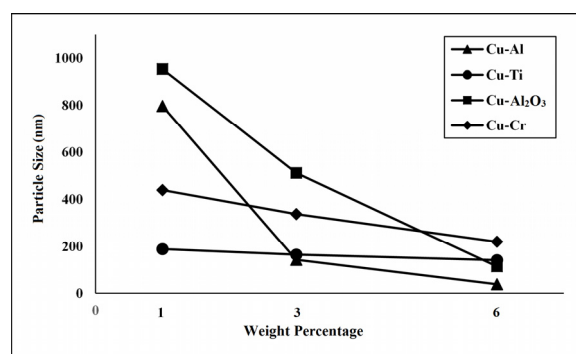


**Fig. 5.** Particle Size Distribution of the synthesized samples.

The morphology and particle size of the powder mixtures are shown in Fig. 6-9. According to Cu-Al images, the particle size decreased by increasing the percentage of aluminum. Generally, particles are completely soft at the start of the milling process, but immediately after the ball milling, these particles welded together and tend to create larger particles [37]. As a consequence, the particles were agglomerated owing to long milling time.

In general, alumina particles by two different mechanisms affect the reduction of powder particle size, first, via incorporating among the copper particles. Second, alumina particles are fractured during the milling process and increase the strain of the lattice. Consequently, the crisp particles of alumina broken by increasing work hardening, and the size of the powder particles reduced [28].

The high cold working by long milling time (90) leads to dissolves of Cr in the Cu lattice. On the other hand, at high chromium percentages, dissolve of Cr in the structure is increased, thereby crisping and fracturing of copper powders are performed. Furthermore, since chromium has a bcc structure, severe cold working causes the creation of static dislocations, which is the origin of the formation of micro-cracks. Other micro-cracks that form at the edge of the powders, and the chromium particles that are dispersed in the lattice, help to create and grow these micro-cracks, and make them open and expand [37]. Therefore, it can be claimed that the higher proportion of the Cr leads to smaller copper composite powders at a constant milling time, and eventually, a fine and uniform structure is obtained by repeated fractures.

Similar to Cu-Cr, due to the long milling time (90 h) of Cu-Ti powder and making a balance between

cold welding and fracture, the particle size distribution is reduced and they also became agglomerated. Titanium particles have an hcp structure and are trapped between copper particles with fcc structure, which have been faster work hardening than copper [27]. At this stage, the more brittle titanium particles are distributed among the softer copper particles and create tiny cracks in their edges. As these cracks grow and spread into the powder grains, failure will occur more rapidly [37]. On the other hand, in the compounds with a higher initial titanium percentage, a richer solid solution is obtained, which is a reason for the higher hardness of these compounds. Hence, the samples with higher titanium content were more fractured and the powder particles, due to the higher hardness by the formation of the richer solid solution, had smaller sizes.



**Fig. 6.** SEM images of Cu-1,3,6wt%Al samples (a,b and c, respectively) after 40 hours of milling.



**Fig. 7.** SEM images of Cu-1,3,6wt%Al$_2$O$_3$ samples (a,b and c, respectively) after 40 hours of milling.
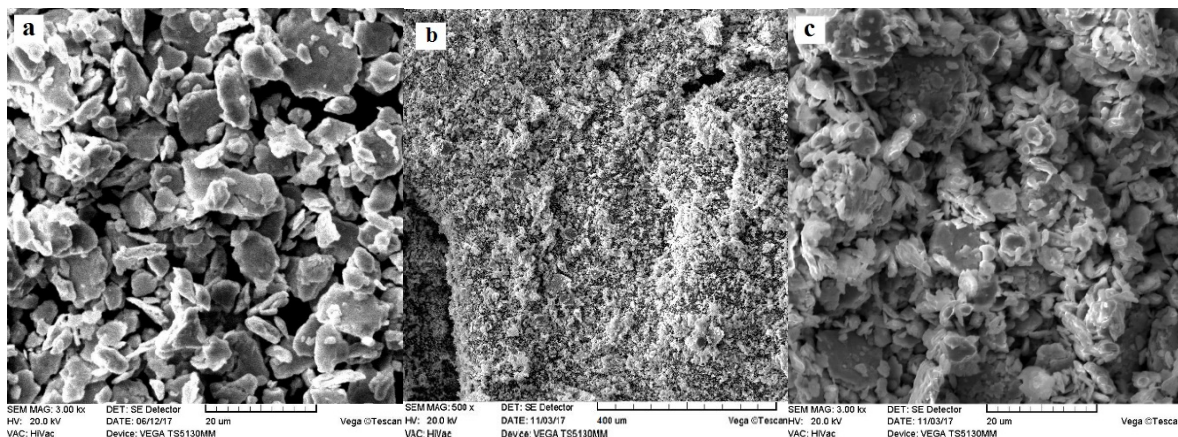


**Fig. 8.** SEM images of Cu-1,3,6wt%Cr samples (a,b and c, respectively) after 90 hours of milling.

6

**Fig. 9.** SEM images of Cu-1,3,6wt%Ti samples (a,b and c, respectively) after 90 hours of milling.

Fig. 10 gives information about the hardness of the samples after annealing at 650 ˚C. Cu-6wt%Ti and Cu-1wt%Al₂O₃ had the highest and lowest micro-hardness, respectively. Due to the high work hardening of the powders at the ball-milling process, the applied force during compression does not cause significant changes in the micro-hardness [37].



**Fig. 10.** Micro-hardness of the samples at different amounts of reinforcement materials.

In all samples, the micro-hardness of the samples is increased by increasing the proportion of the reinforcement materials, which has very well conformity with the results of the lattice strain changes, average crystal size, and lattice constant at the previous analyses. As mentioned earlier, the enhancement amount of reinforcement material leads to an increase in the lattice parameter and micro-hardness. More percentages of alloying elements, the higher density of dislocations and richer solid solution cause to work hardening of copper and so the hardness of the powders increased. The rich solid solution in aging will form a high volume fraction of coherent precipitates, and crystalline

defects provide preferred sites for precipitation. Consequently, these precipitates prevent recovery and recrystallization.

The solubility of titanium in copper is very low at room temperature (0.1 atomic percentage) [42]. In the mechanical alloying of Cu-Ti, the concentration of titanium in the copper matrix is increased and reached more value of the steady-state condition. This super-saturation of Ti in the copper lattice by MA and annealing at 650 ˚C provides a suitable situation for the deposition of titanium atoms in nanometer-sized particles. Therefore, the formation of titanium-rich particles in the matrix of copper in the sintering step at the same time with recovery and recrystallization of the processes, will not only delay the softening process but also halt in many cases. The $Cu_4Ti$ precipitation in the early stages of sintering is in the form of a coherent and fine nanometer [5]. These precipitates which were created on the grain boundaries [43] are obstacles to dislocations movement, thus delays recovery and recrystallization and increases micro-hardness.

Similarly, in Cu-Al and Cu-Cr alloys, like Cu-Ti alloys, the reinforcement element increases the temperature of recrystallization and delays the recovery and recrystallization process. Coherent precipitation of Cu-Al and Cu-Cr which were formed during the aging of the supersaturated solid solution, cause the cease recrystallization and enhancing the hardness.

The electrical resistance changes of the samples are shown in Fig. 11. Cu-1wt%Al and Cu-6wt%Al₂O₃ samples have the highest and lowest electrical resistivity, respectively. The electrical resistance grows by increasing the percentage of the second phase.

7

**Fig. 11.** Electrical resistivity of different samples according to the amount of the reinforcement materials.

According to Matthiessen's rule [44], electrical resistivity $\rho$ of metals expressed by Eq. 1:

$$\rho = \rho_t + \rho_R \tag{1}$$

Where, $\rho_t$ is a contribution of the thermal vibrations and $\rho_R$ is called the residual resistivity and related to the scattering of electrons by impurities and lattice defects (independent of temperature) [45].

$\rho_R$ split up into multiple contributions:

$$\rho_R = \Delta\rho_{im} + \Delta\rho_{gb} \, \Delta\rho_v + \Delta\rho_{dl} + \Delta\rho_{pcl} + \Delta\rho_p \tag{2}$$

Where, these coefficients are related to the following crystallographic factors: $\Delta\rho_{im}$, impurity atoms; $\Delta\rho_{gb}$, grain boundaries; $\Delta\rho_v$, vacancies; $\Delta\rho_{dl}$, dislocations; $\Delta\rho_p$, porosity; and $\Delta\rho_{pcl}$, second-phase particles [45, 46].

After the heat treatment at 650 ˚C, the number of vacancies and dislocations considerably decreased, likewise solid solutions, which decomposed after the annealing stage [45, 47]. Accordingly, just grain boundaries, porosity, and alloying element particles are the major reasons for $\rho_R$.

The higher density of defects (such as solute atoms, grain boundaries, porosities, dislocations, second phases) and the richer solid solution lead to work hardening. As well as, the more weight percentage of the alloying elements provide a high volume of the precipitates. Hence, movements of electrons are prevented and the electrical resistance is grown, by these crystallographic defects and the precipitation. In addition, the role of matrix and the second element in the electrical conductivity of alloys is very important, because their position can affect the electrical conductivity [48].

Cu-Al alloys have the lowest electrical resistivity among all samples and aluminum has less effect on the electrical conductivity of copper than other reinforcement materials. This is owing to the higher conductivity of aluminum than alumina, chromium, and titanium. Conversely, Cu-Al$_2$O$_3$ samples have higher electrical resistance than other samples, because of alumina, which is natural insulation. Deposits of the Al$_2$O$_3$ in the copper act as barriers to the electrons pathway and increase electrical resistance. The main reason for the upward change in electrical resistivity is the lower conductivity of these elements than copper, which has a great effect on electrical conductivity.

Regarding the percentage of the second phase and micro hardness of the samples, electrical resistance in all specimens is very close to the advanced methods for fabrication Cu alloys, such as the report of Uchida et al. [49] by selective laser melting. It seems high capability of the ball-milling to mono-dispersion of the second phase particles cause to strengthen the grain boundaries and better precipitate of the reinforcement materials. On the other hand, the low content solution of alloying elements in the copper lattice has a minor effect on the electrical properties of the copper composites. The comparison of the micro-hardness and the electrical resistivity results represents the maintaining of mechanical strength simultaneous with the proper electrical conductivity of the produced Cu-alloys.

## 4. CONCLUSION

In this study, different Cu-based nanocomposites including Cu-Al, Cu-Al$_2$O$_3$, Cu-Cr, and Cu-Ti were produced by high energy ball-milling. After the heat treatment, their micro-hardness and the crystallographic parameters were compared and studied. The results of XRD analyses show that it is possible to produce nano crystallite size of Cu solid solutions and the crystallite sizes decreased and the internal strain increased by increasing the proportion of the second phase. Adding alumina to the copper lattice has no effect on the copper lattice constant, but by increasing other alloying materials (aluminum, chromium, and titanium), the lattice parameters were affected. According to DLS analysis, the

higher weight percentages of Al, Al$_2$O$_3$, Cr, and Ti lead to smaller particle sizes, and Cu-6wt%Al (38 nm) and Cu-1wt%Al$_2$O$_3$ (954 nm) had the smallest and largest particle size, respectively. Regarding the hardness test, the micro-hardness of all samples is enhanced by increasing the proportion of the reinforcement materials. Accordingly, titanium, and alumina, had the highest and lowest effect on micro-hardness, respectively. The results of electrical resistance indicate that there is a remarkable rise in the electrical resistance by increasing the amount of the second phase and Cu-1wt%Al and Cu-6wt%Al$_2$O$_3$ had the highest and lowest electrical conductivity, respectively.

## ACKNOWLEDGMENT

## 5. REFERENCES

1. Palma, R.H., A. Sepúlveda, R. Espinoza, M.J. Diánez, J.M. Criado, and M.J. Sayagués, "High-temperature deformation of dispersion-strengthened Cu–Zr–Ti–C alloys." Materials Science and Engineering: A, 2005, 391, 60-65.
2. Wang, W., R. Li, C. Zou, Z. Chen, W. Wen, T. Wang, and G. Yin, "Effect of direct current pulses on mechanical and electrical properties of aged Cu–Cr–Zr alloys." Materials & Design, 2016, 92, 135-142.
3. Pellizzari, M. and G. Cipolloni, "Tribological behaviour of Cu based materials produced by mechanical milling/alloying and spark plasma sintering." Wear, 2017, 376, 958-967.
4. Cubberly, W., "Properties and selection: nonferrous alloys and pure metals." Metals Handbook, 1979, 2, 115-117.
5. Datta, A. and W. Soffa, "The structure and properties of age hardened Cu-Ti alloys." Acta Metallurgica, 1976, 24, 987-1001.
6. Fathy, A., A. Wagih, and A. Abu-Oqail, "Effect of ZrO$_2$ content on properties of Cu-ZrO$_2$ nanocomposites synthesized by optimized high energy ball milling." Ceramics International, 2019, 45, 2319-2329.
7. Wagih, A., A. Abu-Oqail, and A. Fathy, "Effect of GNPs content on thermal and mechanical properties of a novel hybrid Cu-Al$_2$O$_3$/GNPs coated Ag nanocomposite." Ceramics International, 2019, 45, 1115-1124.
8. Abu-Oqail, A., A. Samir, A. Essa, A. Wagih, and A. Fathy, "Effect of GNPs coated Ag on microstructure and mechanical properties of Cu-Fe dual-matrix nanocomposite." Journal of Alloys and Compounds, 2019, 781, 64-74.
9. Sadoun, A. and A. Fathy, "Experimental study on tribological properties of Cu–Al$_2$O$_3$ nanocomposite hybridized by graphene nanoplatelets." Ceramics International, 2019, 45, 24784-24792.
10. Fathy, A., "Investigation on microstructure and properties of Cu-ZrO$_2$ nanocomposites synthesized by in situ processing." Materials Letters, 2018, 213, 95-99.
11. Nagarjuna, S., M. Srinivas, K. Balasubramanian, and D. Sarma, "On the variation of mechanical properties with solute content in Cu–Ti alloys." Materials Science and Engineering: A, 1999, 259, 34-42.
12. Eze, A.A., T. Jamiru, E.R. Sadiku, M.O. Durowoju, W.K. Kupolati, I.D. Ibrahim, B.A. Obadele, P.A. Olubambi, and S. Diouf, "Effect of titanium addition on the microstructure, electrical conductivity and mechanical properties of copper by using SPS for the preparation of Cu-Ti alloys." Journal of Alloys and Compounds, 2018, 736, 163-171.
13. Alex, S., K. Chattopadhyay, H.C. Barshilia, and B. Basu, "Thermally evaporated Cu–Al thin film coated flexible glass mirror for concentrated solar power applications." Materials Chemistry and Physics, 2019, 232, 221-228.
14. Lin, Q., Y. Su, M.-J. Zhang, X. Yang, S. Yuan, J. Hu, Y. Lin, J. Liang, and F. Pan, "A novel p-type and metallic dual-functional Cu–Al$_2$O$_3$ ultra-thin layer as the back electrode enabling high performance of thin film solar cells." Chemical Communications, 2016, 52, 10708-10711.

15. De Marco, V., A. Grazioli, and V.M. Sglavo, "Production of planar copper-based anode supported intermediate temperature solid oxide fuel cells cosintered at 950 ˚C." Journal of Power Sources, 2016, 328, 235-240.

16. Gustmann, T., J. Dos Santos, P. Gargarella, U. Kühn, J. Van Humbeeck, and S. Pauly, "Properties of Cu-based shape-memory alloys prepared by selective laser melting." Shape Memory and Superelasticity, 2017, 3, 24-36.

17. Xu, R., Z. Tan, G. Fan, G. Ji, D.-B. Xiong, Q. Guo, Y. Su, Z. Li, and D. Zhang, "High-strength CNT/Al-Zn-Mg-Cu composites with improved ductility achieved by flake powder metallurgy via elemental alloying." Composites Part A: Applied Science and Manufacturing, 2018, 111, 1-11.

18. Elkady, O.A., A. Abu-Oqail, E.M. Ewais, and M. El-Sheikh, "Physico-mechanical and tribological properties of Cu/h-BN nanocomposites synthesized by PM route." Journal of Alloys and Compounds, 2015, 625, 309-317.

19. Rodak, K., "Cu-Cr and Cu-Fe Alloys Processed by New Severe Plastic Deformation: Microstructure and Properties, part 5, Severe Plastic Deformation Techniques, ed. Marcello Cabibbo. InTech, Croatia, 2017, 115.

20. Awadallah, O. and Z. Cheng, "Formation of sol-gel based Cu2ZnSnS4 thin films using ppm-level hydrogen sulfide." Thin Solid Films, 2017, 625, 122-130.

21. Akbari, G. and M. Taghian Dehaqani, "Nanostructure Cu–Cr alloy with high dissolved Cr contents obtained by mechanical alloying process." Powder Metallurgy, 2011, 54, 19-23.

22. Rabiee, M., H. Mirzadeh, and A. Ataie, "Processing of Cu-Fe and Cu-Fe-SiC nanocomposites by mechanical alloying." Advanced Powder Technology, 2017, 28, 1882-1887.

23. Cheng, J., Q. Cai, B. Zhao, S. Yang, F. Chen, and B. Li, "Microstructure and Mechanical Properties of Nanocrystalline Al-Zn-Mg-Cu Alloy Prepared by Mechanical Alloying and Spark Plasma Sintering." Materials, 2019, 12, 1255.

24. Abu-Oqail, A., A. Wagih, A. Fathy, O. Elkady, and A. Kabeel, "Effect of high energy ball milling on strengthening of Cu-ZrO$_2$ nanocomposites." Ceramics International, 2019, 45, 5866-5875.

25. Wagih, A., A. Fathy, and A. Kabeel, "Optimum milling parameters for production of highly uniform metal-matrix nanocomposites with improved mechanical properties." Advanced Powder Technology, 2018, 29, 2527-2537.

26. Torabi, A., R. Babaheydari, G. Akbari, and S. Mirabootalebi, "Optimizing of micro-hardness of nanostructured Cu–Cr solid solution produced by mechanical alloying using ANN and genetic algorithm." SN Applied Sciences, 2020, 2, 1-9.

27. Pourfereidouni, A. and G.H. Akbari. Development of Nano-Structure Cu-Ti Alloys by Mechanical Alloying Process. in Advanced Materials Research. 2013, 829, 168-172.

28. Safi, S. and G. Akbari, "Evaluation of Synthesizing Al$_2$O$_3$ Nano Particles in Copper Matrix by Mechanical Alloying of Cu-1% Al and Copper Oxide." Journal of Advanced Materials in Engineering (Esteghlal), 2017, 36, 71-85.

29. Akbari, G.H. and D.M. TAGHIAN, "Behavior of cu-cr powder mixtures during mechanical alloying." International Journal of Engineering, 2010, 23, 69-76.

30. Galluzzo, M.D., J.A. Maslyn, D.B. Shah, and N.P. Balsara, "Ohm's law for ion conduction in lithium and beyond-lithium battery electrolytes." The Journal of chemical physics, 2019, 151, 104502.

31. H. Okamoto., M.E. Schlesinger., E.M. Mueller., Alloy Phase Diagrams, part 3, ASM Handbook, Materials Park, Ohio, USA, 1992, 285.

32. Bhanumurthy, K., D. Joyson, S. Jawale, A. Laik, and G. Dey, "Diffusion bonding of nuclear materials." BARC Newsl, 2013, 331, 19-25.

33. Zeng, K. and M. Hämäläinen, "Thermodynamic analysis of stable and metastable equilibria in the Cu-Cr system." Calphad, 1995, 19, 93-104.

34. Li, J., X. Bi, X. Geng, R. Hu, and H. Fu, "Study on the in situ composites microstructure of the directionally solidified hypoeutectic Cu–Cr alloys." Journal of materials science, 2004, 39, 4933-4935.

35. Soffa, W. and D. Laughlin, "High-strength age hardening copper–titanium alloys: redivivus." Progress in Materials Science, 2004, 49, 347-366.

36. Babaheydari, R., S. Mirabootalebi, and G. Akbari, "Investigation on Mechanical and Electrical Properties of Cu-Ti Nanocomposite Produced by Mechanical Alloying." International Journal of Engineering, 2020, 33, 1759-1765.

37. Suryanarayana, C., Mechanical alloying and milling, Progress in materials science, Elsevier, USA, 2001, 1-184.

38. Sheibani, S., S. Heshmati-Manesh, and A. Ataie, "Structural investigation on nano-crystalline Cu–Cr supersaturated solid solution prepared by mechanical alloying." Journal of Alloys and Compounds, 2010, 495, 59-62.

39. Eckert, J., J. Holzer, C. Krill, and W. Johnson, "Structural and thermodynamic properties of nanocrystalline fcc metals prepared by mechanical attrition." Journal of Materials Research, 1992, 7, 1751-1761.

40. Akbari, G.H. and D.M. TAGHIAN, "Behavior of cu-cr powder mixtures during mechanical alloying." International Journal of Engineering, 2010, 23, 69-76.

41. Li, Z., A. Samuel, F. Samuel, C. Ravindran, and S. Valtierra, "Effect of alloying elements on the segregation and dissolution of CuAl 2 phase in Al-Si-Cu 319 alloys." Journal of materials science, 2003, 38, 1203-1218.

42. Murray, J., "The Cu− Ti (copper-titanium) system." Bulletin of alloy phase diagrams, 1983, 4, 81-95.

43. Lopez-Hirata, V.M., F. Hernandez-Santiago, M.L. Saucedo-Muñoz, E.O. Avila-Davila, and J.D. Villegas-Cardenas, Analysis of β′(Cu4Ti) Precipitation During Isothermal Aging of a Cu–4 wt% Ti Alloy, part 11, Characterization of Minerals, Metals, and Materials, ed. Jian Li. Springer, 2020, 403-412.

44. Glasbrenner, J.K., B.S. Pujari, and K.D. Belashchenko, "Deviations from Matthiessen's rule and resistivity saturation effects in Gd and Fe from first principles." Physical Review B, 2014, 89, 174408.

45. Wang, Y., G. Bosse, H. Nair, N. Schreiber, J. Ruf, B. Cheng, C. Adamo, D. Shai, Y. Lubashevsky, and D. Schlom, "Sub-THz momentum drag and violation of Matthiessen's rule in an ultraclean ferromagnetic SrRuOmetallic thin film." ArXiv, 2020, 1, 1-12.

46. Botcharova, E., J. Freudenberger, and L. Schultz, "Mechanical and electrical properties of mechanically alloyed nanocrystalline Cu–Nb alloys." Acta materialia, 2006, 54, 3333-3341.

47. Gangulee, A., "The structure of electroplated and vapor-deposited copper films." Journal of Applied Physics, 1972, 43, 867-873.

48. Botcharova, E., J. Freudenberger, and L. Schultz, "Cu–Nb alloys prepared by mechanical alloying and subsequent heat treatment." Journal of alloys and compounds, 2004, 365, 157-163.

49. Şimşek, I., "Investigation of the effect of second phase precipitates on the corrosion and electrical conductivity of 7075 aluminum alloys." Anti-Corrosion Methods and Materials, 2019, 66, 683-688.

50. Uchida, S., T. Kimura, T. Nakamoto, T. Ozaki, T. Miki, M. Takemura, Y. Oka, and R. Tsubota, "Microstructures and electrical and mechanical properties of Cu-Cr alloys fabricated by selective laser melting." Materials & Design, 2019, 175, 107815.